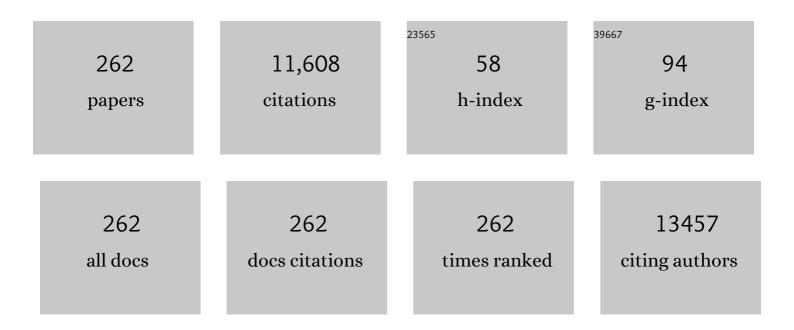
## **Changsheng Xie**

List of Publications by Year in descending order

Source: https://exaly.com/author-pdf/58927/publications.pdf Version: 2024-02-01



#	Article	IF	CITATIONS
1	Exposed Mo atoms induced by micropores enhanced H2S sensing of MoO3 nanoflowers. Journal of Hazardous Materials, 2022, 429, 128270.	12.4	22
2	Active W Sites Promoted by Defect Engineering Enhanced C <sub>2</sub> H <sub>6</sub> S <sub>3</sub> Sensing Performance of WO <sub>3</sub> Nanosheets. ACS Sensors, 2022, 7, 1894-1902.	7.8	13
3	Inhomogeneous oxidation of ultrathin SnS2 nanoflowers and its effect on low–temperatures NO2 gas sensing. Applied Surface Science, 2022, 601, 154213.	6.1	5
4	Two-Dimensional Mesoporous WO3 Nanosheets for Detection of Dimethyl Trisulfide. IEEE Sensors Journal, 2021, , 1-1.	4.7	0
5	SW-WAL: Leveraging Address Remapping of SSDs to Achieve Single-Write Write-Ahead Logging. , 2021, , .		0
6	Modeling of Threshold Voltage Distribution in 3D NAND Flash Memory. , 2021, , .		12
7	A universal strategy for the synthesis of porous two-dimensional transition metal oxide nanosheets based on chemical topology transformation. Science China Materials, 2021, 64, 2477-2485.	6.3	5
8	Exploiting Resistance Drift Characteristics to Improve Reliability of LDPC-Assisted Phase-Change Memory. IEEE Transactions on Device and Materials Reliability, 2021, 21, 324-330.	2.0	2
9	Selectivity of a ZnO@ZIF-71@PDMS Nanorod Array Gas Sensor Enhanced by Coating a Polymer Selective Separation Membrane. ACS Applied Materials & amp; Interfaces, 2021, 13, 54589-54596.	8.0	18
10	Intelligent Prediction of Flash Lifetime via Online Domain Adaptation. , 2021, , .		1
11	Highly sensitive and ultralow detection limit of room-temperature NO2 sensors using in-situ growth of PPy on mesoporous NiO nanosheets. Organic Electronics, 2020, 77, 105504.	2.6	18
12	Catalytic Activation of Cobalt Doping Sites in ZIF-71-Coated ZnO Nanorod Arrays for Enhancing Gas-Sensing Performance to Acetone. ACS Applied Materials & Interfaces, 2020, 12, 48948-48956.	8.0	47
13	BeLDPC: Bit Errors Aware Adaptive Rate LDPC Codes for 3D TLC NAND Flash Memory. , 2020, , .		9
14	Mechanistic study of N–H- and H–N-codoping of a TiO <sub>2</sub> photocatalyst for efficient degradation of benzene under visible light. RSC Advances, 2020, 10, 2757-2766.	3.6	10
15	Synthesis of core-shell flower-like WO3@ZIF-71 with enhanced response and selectivity to H2S gas. Solid State Ionics, 2020, 350, 115278.	2.7	27
16	Molecular sieving property adjusted by the encapsulation of Ag nanoparticles into ZnO@ZIF-71 nanorod arrays. Chemical Communications, 2019, 55, 11045-11048.	4.1	7
17	A facile low-temperature synthesis of hierarchical porous Co <sub>3</sub> O <sub>4</sub> micro/nano structures derived from ZIF-67 assisted by ammonium perchlorate. Inorganic Chemistry Frontiers, 2019, 6, 715-722.	6.0	68
18	High-Adhesion Stretchable Electrode via Cross-Linking Intensified Electroless Deposition on a Biomimetic Elastomeric Micropore Film. ACS Applied Materials & Interfaces, 2019, 11, 20535-20544.	8.0	33

#	Article	IF	CITATIONS
19	High selectivity for room temperature detection of ammonia via in-situ Raman spectroscopy based on Pt quantum dots modified WS2 nanosheets. Applied Surface Science, 2019, 485, 22-28.	6.1	11
20	Gas Adsorption at Metal Sites for Enhancing Gas Sensing Performance of ZnO@ZIF-71 Nanorod Arrays. Langmuir, 2019, 35, 3248-3255.	3.5	40
21	Effect of Heterointerface on NO2 Sensing Properties of In-Situ Formed TiO2 QDs-Decorated NiO Nanosheets. Nanomaterials, 2019, 9, 1628.	4.1	8
22	Structure evolution from Prussian-blue nanocubes to hollow nanocage composites <i>via</i> sodium tungstate etching. Chemical Communications, 2019, 55, 13386-13389.	4.1	13
23	Multilevel Microstructured Flexible Pressure Sensors with Ultrahigh Sensitivity and Ultrawide Pressure Range for Versatile Electronic Skins. Small, 2019, 15, e1804559.	10.0	163
24	Enhanced room-temperature NH3 gas sensing by 2D SnS2 with sulfur vacancies synthesized by chemical exfoliation. Sensors and Actuators B: Chemical, 2018, 262, 771-779.	7.8	140
25	Pore size dependent gas-sensing selectivity based on ZnO@ZIF nanorod arrays. Sensors and Actuators B: Chemical, 2018, 258, 1099-1106.	7.8	134
26	CulnS2 QDs decorated ring-like NiO for significantly enhanced room-temperature NO2 sensing performances via effective interfacial charge transfer. Sensors and Actuators B: Chemical, 2018, 256, 1001-1010.	7.8	18
27	Preparing high-adhesion silver coating on APTMS modified polyethylene with excellent anti-bacterial performance. Applied Surface Science, 2018, 436, 117-124.	6.1	21
28	Metal–Organic Framework-Assisted Construction of TiO <sub>2</sub> /Co <sub>3</sub> O <sub>4</sub> Highly Ordered Necklace-like Heterostructures for Enhanced Ethanol Vapor Sensing Performance. Langmuir, 2018, 34, 14577-14585.	3.5	42
29	Red Phosphorus: An Elementary Semiconductor for Room-Temperature NO <sub>2</sub> Gas Sensing. ACS Sensors, 2018, 3, 2629-2636.	7.8	19
30	A Low ost Polyaniline@Textileâ€Based Multifunctional Sensor for Simultaneously Detecting Tactile and Olfactory Stimuli. Macromolecular Materials and Engineering, 2018, 303, 1800340.	3.6	16
31	Tuning the Particle Size of Prussian Blue by a Dual Anion Source Method. Crystal Growth and Design, 2018, 18, 5780-5789.	3.0	18
32	Two-dimensional WS2-based nanosheets modified by Pt quantum dots for enhanced room-temperature NH3 sensing properties. Applied Surface Science, 2018, 455, 45-52.	6.1	77
33	Quantitative characterization of the long-term charge storage of a ZnO-based nanorod array film through persistent photoconductance. RSC Advances, 2018, 8, 16455-16463.	3.6	11
34	Metal-oxide-semiconductor based gas sensors: screening, preparation, and integration. Physical Chemistry Chemical Physics, 2017, 19, 6313-6329.	2.8	400
35	Effect of layer number on recovery rate of WS 2 nanosheets for ammonia detection at room temperature. Applied Surface Science, 2017, 414, 244-250.	6.1	107
36	A novel exposed facet dependent topological transformation mechanism from hydrozincite microspheres into hierarchical mesoporous ZnO structures. Materials Letters, 2017, 202, 142-145.	2.6	5

#	Article	IF	CITATIONS
37	Highly responsive chemical sensing on NO 2 at room temperature based on reduced porous graphene. Materials Letters, 2017, 204, 27-30.	2.6	12
38	Temperature & light modulation to enhance the selectivity of Pt-modified zinc oxide gas sensor. Sensors and Actuators B: Chemical, 2017, 247, 903-915.	7.8	41
39	Enhancing room-temperature NO2 sensing properties via forming heterojunction for NiO-rGO composited with SnO2 nanoplates. Sensors and Actuators B: Chemical, 2017, 243, 1010-1019.	7.8	78
40	Origin of the efficient catalytic thermal decomposition of ammonium perchlorate over (2â^1â^10) facets of ZnO nanosheets: surface lattice oxygen. RSC Advances, 2017, 7, 40262-40269.	3.6	18
41	2D WS2 nanosheets with TiO2 quantum dots decoration for high-performance ammonia gas sensing at room temperature. Sensors and Actuators B: Chemical, 2017, 253, 1034-1042.	7.8	128
42	Enhanced visible-light photocatalytic performance of highly-dispersed Pt/g-C <sub>3</sub> N <sub>4</sub> nanocomposites by one-step solvothermal treatment. RSC Advances, 2017, 7, 33552-33557.	3.6	36
43	Porous LaFeO3/SnO2 nanocomposite film for CO2 detection with high sensitivity. Materials Chemistry and Physics, 2017, 186, 228-236.	4.0	45
44	BiOCl/TiO2 heterojunction network with high energy facet exposed for highly efficient photocatalytic degradation of benzene. Applied Surface Science, 2017, 396, 590-598.	6.1	50
45	In situ synthesis of C-TiO2/g-C3N4 heterojunction nanocomposite as highly visible light active photocatalyst originated from effective interfacial charge transfer. Applied Catalysis B: Environmental, 2017, 202, 489-499.	20.2	262
46	Fast identification of CO by using single Pt-modified WO3 sensing film based on optical modulation. Sensors and Actuators B: Chemical, 2016, 232, 506-513.	7.8	19
47	Charge separation in branched TiO2 nanorod array homojunction aroused by quantum effect for enhanced photocatalytic decomposition of gaseous benzene. Applied Surface Science, 2016, 389, 165-172.	6.1	29
48	The irreversible R-T curves of metal oxide gas sensor under programmed temperature cycle. Sensors and Actuators B: Chemical, 2016, 235, 481-491.	7.8	22
49	Facile synthesis of diverse graphene nanomeshes based on simultaneous regulation of pore size and surface structure. Scientific Reports, 2016, 6, 32310.	3.3	23
50	A method for modeling and deciphering the persistent photoconductance and long-term charge storage of ZnO nanorod arrays. Nano Research, 2016, 9, 2972-3002.	10.4	21
51	Enhanced room temperature NO <sub>2</sub> response of NiO–SnO <sub>2</sub> nanocomposites induced by interface bonds at the p–n heterojunction. Physical Chemistry Chemical Physics, 2016, 18, 5386-5396.	2.8	47
52	The microstructure, stoichiometric ratio and room temperature ferromagnetic properties of V-doped ZnO films deposited at different substrate temperatures. Journal of Materials Science: Materials in Electronics, 2016, 27, 163-170.	2.2	3
53	A modular calcination method to prepare modified N-doped TiO 2 nanoparticle with high photocatalytic activity. Applied Catalysis B: Environmental, 2016, 183, 308-316.	20.2	116
54	Effect of Nickel Vacancies on the Room-Temperature NO <sub>2</sub> Sensing Properties of Mesoporous NiO Nanosheets. Journal of Physical Chemistry C, 2016, 120, 3936-3945.	3.1	129

#	Article	IF	CITATIONS
55	Modeling the In-home Lifestyle of Chronic Anorectal Patients via a Sensing Home. Lecture Notes in Computer Science, 2016, , 188-199.	1.3	1
56	Sensing Home: A Cost-Effective Design for Smart Home via Heterogeneous Wireless Networks. Sensors, 2015, 15, 30270-30292.	3.8	16
57	Temperature-dependent photothermocatalytic mineralization of gaseous benzene based on rutile TiO2 nanorod array. Materials Letters, 2015, 139, 336-339.	2.6	6
58	A Novel Kind of Green Solid Propellant Containing H2O2Cured at Room Temperature (SPHP). Propellants, Explosives, Pyrotechnics, 2015, 40, 772-778.	1.6	2
59	Synchronously Deriving Electron Concentration and Mobility by Temperature- and Oxygen-Dependent Conductivity of Porous ZnO Nanocrystalline Film. Journal of Physical Chemistry C, 2015, 119, 695-702.	3.1	7
60	Enhanced gas sensing performance of Li-doped ZnO nanoparticle film by the synergistic effect of oxygen interstitials and oxygen vacancies. Applied Surface Science, 2015, 330, 126-133.	6.1	79
61	Fabrication and different photoelectric responses of nanocrystalline ZnO film irradiated with UV and white light in dry air. Applied Physics A: Materials Science and Processing, 2015, 120, 1299-1307.	2.3	3
62	A novel headspace integrated E-nose and its application in discrimination of Chinese medical herbs. Sensors and Actuators B: Chemical, 2015, 221, 556-563.	7.8	47
63	Effect of Grain-Boundaries in NiO Nanosheet Layers Room-Temperature Sensing Mechanism under NO <sub>2</sub> . Journal of Physical Chemistry C, 2015, 119, 17930-17939.	3.1	60
64	Graphene-wrapped WO3 nanospheres with room-temperature NO2 sensing induced by interface charge transfer. Sensors and Actuators B: Chemical, 2015, 220, 201-209.	7.8	91
65	Interface Bonds Determined Gas-Sensing of SnO <sub>2</sub> –SnS <sub>2</sub> Hybrids to Ammonia at Room Temperature. ACS Applied Materials & Interfaces, 2015, 7, 11359-11368.	8.0	191
66	CdS/TiO2 nanocomposite film and its enhanced photoelectric responses to dry air and formaldehyde induced by visible light at room temperature. Journal of Alloys and Compounds, 2015, 645, 17-23.	5.5	37
67	Room temperature NO <sub>2</sub> sensing: what advantage does the rGO–NiO nanocomposite have over pristine NiO?. Physical Chemistry Chemical Physics, 2015, 17, 14903-14911.	2.8	59
68	Through-Process Analytical Modeling of Photoconductance Spectrum for Porous ZnO Nanocrystalline Film. Chemistry of Materials, 2015, 27, 2861-2874.	6.7	8
69	Surface doping of La ions into ZnO nanocrystals to lower the optimal working temperature for HCHO sensing properties. Physical Chemistry Chemical Physics, 2015, 17, 27437-27445.	2.8	61
70	Hierarchical ZnO hollow microspheres with exposed (001) facets as promising catalysts for the thermal decomposition of ammonium perchlorate. CrystEngComm, 2015, 17, 8689-8696.	2.6	26
71	Assessing multi-variable coupling effects of UV illumination, heat and oxygen on porous ZnO nanocrystalline film through electron concentration and mobility extraction. Physical Chemistry Chemical Physics, 2015, 17, 18045-18054.	2.8	6
72	Competitive influence of surface area and mesopore size on gas-sensing properties of SnO2 hollow fibers. Journal of Materials Science, 2015, 50, 7725-7734.	3.7	15

#	Article	IF	CITATIONS
73	Optimizing the packing density of TiO <sub>2</sub> nanorod arrays for enhanced light harvesting by a light trapping effect and its photocatalytic decomposition of gaseous benzene. CrystEngComm, 2015, 17, 1151-1158.	2.6	27
74	Highly efficient visible-light driven photocatalyst with enhanced charge separation prepared by annealing continuously in ammonia and vacuum. Applied Catalysis B: Environmental, 2015, 166-167, 1-8.	20.2	16
75	A novel method in the gas identification by using WO3 gas sensor based on the temperature-programmed technique. Sensors and Actuators B: Chemical, 2015, 206, 220-229.	7.8	29
76	Alterations in the endometrium of rats, rabbits, and Macaca mulatta that received an implantation of copper/low-density polyethylene nanocomposite. International Journal of Nanomedicine, 2014, 9, 1127.	6.7	8
77	A novel planar integration of all-solid-state capacitor and photodetector by an ultra-thin transparent sulfated TiO 2 film. Nano Energy, 2014, 9, 252-263.	16.0	20
78	Fabrication of porous TiO <sub>2</sub> –SiO <sub>2</sub> multifunctional anti-reflection coatings by sol–gel spin coating method. RSC Advances, 2014, 4, 58101-58107.	3.6	17
79	Comparative study on the visible light driven photocatalytic activity between substitutional nitrogen doped TiO2. Applied Catalysis A: General, 2014, 488, 239-247.	4.3	34
80	Gas-sensing properties and in situ diffuse reflectance infrared Fourier transform spectroscopy study of formaldehyde adsorption and reactions on SnO2 films. Journal of Materials Research, 2014, 29, 139-147.	2.6	8
81	Tin oxide thick film by doping rare earth for detecting traces of CO2: Operating in oxygen-free atmosphere. Materials Research Bulletin, 2014, 52, 56-64.	5.2	19
82	Highly sensitive porous metal oxide films for early detection of electrical fire: Surface modification and high throughput screening. Sensors and Actuators B: Chemical, 2014, 191, 431-437.	7.8	8
83	Direct experimental evidence for SbZn–2VZn complex as the important defect in the Sb-doped ZnO nanocrystals. Materials Letters, 2014, 116, 363-366.	2.6	17
84	Enhanced response to NO2 with CuO/ZnO laminated heterostructured configuration. Sensors and Actuators B: Chemical, 2014, 195, 500-508.	7.8	33
85	Gas sensing properties and in situ diffuse reflectance infrared Fourier transform spectroscopy study of trichloroethylene adsorption and reactions on SnO2 films. Applied Surface Science, 2014, 300, 98-103.	6.1	10
86	Study on the structure and properties of core–shell Fe/Al composite powder synthesized by MOCVD in fluidized bed. Advanced Powder Technology, 2014, 25, 676-681.	4.1	10
87	A comparative study of microstructures on the photoelectric properties of tungsten trioxide films with plate-like arrays. Applied Surface Science, 2014, 297, 116-124.	6.1	23
88	Selectively enhanced UV and NIR photoluminescence from a degenerate ZnO nanorod array film. Journal of Materials Chemistry C, 2014, 2, 4566.	5.5	104
89	Anti-aging properties of the Cu/LDPE composite for intrauterine contraceptive devices. Composites Science and Technology, 2014, 90, 139-146.	7.8	9
90	An efficient method to modulate the structure, morphology and properties of WO3 through niobium doping. Journal of Alloys and Compounds, 2014, 610, 132-137.	5.5	30

#	Article	IF	CITATIONS
91	Synthesis and characterization of NiO/TiO2 porous films and their photocurrent-enhanced mechanism in gas phase. Journal of Alloys and Compounds, 2014, 584, 356-362.	5.5	5
92	Temperature―and Atmosphereâ€Dependent Defect Chemistry Model of <scp><scp>SnO</scp></scp> <sub>2</sub> Nanocrystalline Film. Journal of the American Ceramic Society, 2014, 97, 2091-2098.	3.8	9
93	The coupled effect of oxygen vacancies and Pt on the photoelectric response of tungsten trioxide films. Journal of Materials Chemistry C, 2014, 2, 9467-9477.	5.5	35
94	The atomic origin of high catalytic activity of ZnO nanotetrapods for decomposition of ammonium perchlorate. CrystEngComm, 2014, 16, 570-574.	2.6	43
95	Fabrication of TiO2rod in tube nanostructure with enhanced photocatalytic activity: investigation of the effect of the states of the precursor on morphology. RSC Advances, 2014, 4, 36708.	3.6	8
96	Defect Chemistry of the Metal Cation Defects in the p- and n-Doped SnO2 Nanocrystalline Films. Journal of Physical Chemistry C, 2014, 118, 18097-18109.	3.1	49
97	Mechanistic Insights into Formation of SnO <sub>2</sub> Nanotubes: Asynchronous Decomposition of Poly(vinylpyrrolidone) in Electrospun Fibers during Calcining Process. Langmuir, 2014, 30, 11183-11189.	3.5	53
98	Correlation between microstructure and gas sensing properties of hierarchical porous tin oxide topologically synthesized on coplanar sensors' surface. Sensors and Actuators B: Chemical, 2014, 205, 416-425.	7.8	20
99	Temperature-Programmed Technique Accompanied with High-Throughput Methodology for Rapidly Searching the Optimal Operating Temperature of MOX Gas Sensors. ACS Combinatorial Science, 2014, 16, 459-465.	3.8	11
100	Synthesis of a novel N H TiO 2 photocatalyst by annealing in NH 3 and H 2 for complete decomposition of high concentration benzene under visible light irradiation. Materials Letters, 2014, 136, 258-261.	2.6	10
101	A novel approach to fabricate metal oxide nanowire-like networks based coplanar gas sensors array for enhanced selectivity. Sensors and Actuators B: Chemical, 2014, 204, 351-359.	7.8	38
102	2-Methyl-2,4-pentanediol gas sensor properties of nano-SnO2 flat-type coplanar gas sensing arrays at low detection limit. Materials Science-Poland, 2014, 32, 181-187.	1.0	1
103	Controlled surface modification of various substrates with SnO <sub>2</sub> nanoparticles. CrystEngComm, 2014, 16, 139-143.	2.6	5
104	Catalytic oxidation of formaldehyde on surface of HTiO2/HCTiO2 without light illumination at room temperature. Applied Catalysis B: Environmental, 2014, 147, 490-498.	20.2	106
105	ZnO Micro/Nanocrystals with Tunable Exposed (0001) Facets for Enhanced Catalytic Activity on the Thermal Decomposition of Ammonium Perchlorate. Journal of Physical Chemistry C, 2014, 118, 11833-11841.	3.1	95
106	Mg-doped SiO2 porous coating with high anti-reflection in the visible spectrum. Materials Letters, 2014, 132, 214-217.	2.6	1
107	The influence of Au and Pt electrodes on the stability of TiO2 under UV light activation for sensing formaldehyde in moisture circumstances. Sensors and Actuators B: Chemical, 2014, 199, 15-21.	7.8	17
108	Al-doping induced formation of oxygen-vacancy for enhancing gas-sensing properties of SnO2 NTs by electrospinning. Sensors and Actuators B: Chemical, 2014, 198, 62-69.	7.8	107

#	Article	IF	CITATIONS
109	Highly photoactive sensor based on NiO modified TiO2 porous film for diethyl ether. Sensors and Actuators B: Chemical, 2014, 195, 439-445.	7.8	31
110	Comparative study of ZnO nanorod array and nanoparticle film in photoelectric response and charge storage. Journal of Alloys and Compounds, 2014, 585, 267-276.	5.5	33
111	Hierarchical porous SnO2 micro-rods topologically transferred from tin oxalate for fast response sensors to trace formaldehyde. Sensors and Actuators B: Chemical, 2014, 190, 585-592.	7.8	87
112	UV light activation of TiO2 for sensing formaldehyde: How to be sensitive, recovering fast, and humidity less sensitive. Sensors and Actuators B: Chemical, 2014, 202, 964-970.	7.8	75
113	Quantitative Detection of Molds Counts in Cigarette Cut Tobacco at Early Stages by an Electronic Nose. Sensor Letters, 2014, 12, 56-63.	0.4	2
114	Extraordinarily enhanced gas phase photoelectric response of CdS/TiO2 nanocomposite photoelectrode: CdS as a sensitizer and a hole capturer. Journal of Nanoparticle Research, 2013, 15, 1.	1.9	3
115	Laser cladding of Zr-based coating on AZ91D magnesium alloy for improvement of wear and corrosion resistance. Bulletin of Materials Science, 2013, 36, 99-105.	1.7	18
116	Preparation and gas-sensing property of parallel-aligned ZnO nanofibrous films. Bulletin of Materials Science, 2013, 36, 505-511.	1.7	5
117	Preparation and photocatalytic activity of TiO2/CeO2/Bi2O3 composite for Rhodamine B degradation under visible light irradiation. Journal of Alloys and Compounds, 2013, 581, 385-391.	5.5	31
118	Full mineralization of toluene by photocatalytic degradation with porous TiO2/SiC nanocomposite film. Journal of Alloys and Compounds, 2013, 552, 504-510.	5.5	55
119	CdS/ZnO nanocomposite film and its enhanced photoelectric response to UV and visible lights at low bias. Sensors and Actuators B: Chemical, 2013, 188, 1158-1166.	7.8	37
120	Pore-size-dependent sensing property of hierarchical SnO2 mesoporous microfibers as formaldehyde sensors. Sensors and Actuators B: Chemical, 2013, 186, 640-647.	7.8	64
121	Influence of pore morphology on the mechanical properties of Cu/LDPE porous composites for intrauterine devices. Materials Letters, 2013, 93, 275-277.	2.6	3
122	Synthesis of Al/Fe3Al core–shell intermetallic nanoparticles by chemical liquid deposition method. Advanced Powder Technology, 2013, 24, 926-931.	4.1	9
123	Characterization of Incidental Photon-to-electron Conversion Efficiency (IPCE) of porous TiO2/SnO2 composite film. Journal of Alloys and Compounds, 2013, 569, 88-94.	5.5	29
124	An In2O3 nanowire-like network fabricated on coplanar sensor surface by sacrificial CNTs for enhanced gas sensing performance. Sensors and Actuators B: Chemical, 2013, 185, 345-353.	7.8	46
125	Enhancement of photocatalytic property of ZnO for gaseous formaldehyde degradation by modifying morphology and crystal defect. Journal of Alloys and Compounds, 2013, 550, 190-197.	5.5	51
126	Conduction model of coupled domination by bias and neck for porous films as gas sensor. Sensors and Actuators B: Chemical, 2013, 176, 217-224.	7.8	12

#	Article	IF	CITATIONS
127	In situ diffuse reflectance infrared Fourier transform spectroscopy study of formaldehyde adsorption and reactions on nano γ-Fe2O3 films. Applied Surface Science, 2013, 270, 405-410.	6.1	35
128	La2O3-sensitized SnO2 nanocrystalline porous film gas sensors and sensing mechanism toward formaldehyde. Sensors and Actuators B: Chemical, 2013, 188, 137-146.	7.8	70
129	Preparation and cupric ion release behavior of Cu/LDPE porous composites with tunable pore morphology for intrauterine devices. Materials Science and Engineering C, 2013, 33, 2800-2807.	7.3	3
130	Processing–microstructure–property correlations of gas sensors based on ZnO nanotetrapods. Sensors and Actuators B: Chemical, 2013, 181, 509-517.	7.8	28
131	Chitosan/alginate multilayer film for controlled release of IDM on Cu/LDPE composite intrauterine devices. Colloids and Surfaces B: Biointerfaces, 2013, 109, 82-89.	5.0	19
132	Specially environmental responses induced by multi-field coupling for nanocrystalline SnO2 porous film as gas sensor. Sensors and Actuators B: Chemical, 2013, 182, 239-249.	7.8	8
133	Enhanced Photocatalytic Activity of Chemically Bonded TiO <sub>2</sub> /Graphene Composites Based on the Effective Interfacial Charge Transfer through the C–Ti Bond. ACS Catalysis, 2013, 3, 1477-1485.	11.2	461
134	A low temperature gas sensor based on Pd-functionalized mesoporous SnO2 fibers for detecting trace formaldehyde. RSC Advances, 2013, 3, 11823.	3.6	63
135	A full-sunlight-driven photocatalyst with super long-persistent energy storage ability. Scientific Reports, 2013, 3, 2409.	3.3	86
136	Nanoscale SnO <sub>2</sub> Flat-Type Coplanar Hexanal Gas Sensor Arrays at ppb Level. Journal of Nanoscience and Nanotechnology, 2013, 13, 4370-4374.	0.9	8
137	Characteristics of Al-doped ZnO thin films prepared in Ar + H2 atmosphere and their vacuum annealing behavior. Journal of Vacuum Science and Technology A: Vacuum, Surfaces and Films, 2013, 31, .	2.1	11
138	In Situ Diffuse Reflectance Fourier Transform Infrared Spectroscopy (DRIFTS) Study of Formaldehyde Adsorption and Reactions on Pd-Doped Nano–γ-Fe <sub>2</sub> O <sub>3</sub> Films. Applied Spectroscopy, 2013, 67, 930-939.	2.2	8
139	Biological Evaluation of the Copper/Low-density Polyethylene Nanocomposite Intrauterine Device. PLoS ONE, 2013, 8, e74128.	2.5	10
140	Fabrication and Hexanal Gas Sensing Property of Nano-SnO2 Flat-type Coplanar Gas Sensor Arrays at Ppb Level. Current Nanoscience, 2013, 9, 357-362.	1.2	7
141	Room temperature formaldehyde sensors with enhanced performance, fast response and recovery based on zinc oxide quantum dots/graphene nanocomposites. Nanoscale, 2012, 4, 5651.	5.6	223
142	High Sensitivity and Selectivity of C-Doped \${m WO}_{3}\$ Gas Sensors Toward Toluene and Xylene. IEEE Sensors Journal, 2012, 12, 2209-2214.	4.7	45
143	High Photoconductive Response of Gas-Sensitized Porous Nanocrystalline TiO <sub>2</sub> Film in Formaldehyde Ambience and Carrier Transport Kinetics. Journal of Physical Chemistry C, 2012, 116, 19673-19681.	3.1	18
144	New insights into the relationship between photocatalytic activity and photocurrent of TiO2/WO3 nanocomposite. Applied Catalysis A: General, 2012, 433-434, 81-87.	4.3	82

#	Article	IF	CITATIONS
145	MOX (M=Zn, Co, Fe)/AP shell–core nanocomposites for self-catalytical decomposition of ammonium perchlorate. Journal of Alloys and Compounds, 2012, 513, 213-219.	5.5	61
146	A study of photocurrent spectrum of porous ZnO film sensitized by metal chloride solutions. Applied Surface Science, 2012, 263, 465-470.	6.1	7
147	Reaction characteristics of nano-aluminum and water by in-situ investigation. Materials Chemistry and Physics, 2012, 136, 466-471.	4.0	8
148	Chemically bonded graphene/BiOCl nanocomposites as high-performance photocatalysts. Physical Chemistry Chemical Physics, 2012, 14, 10572.	2.8	129
149	Preparation of Fe/Al Composites with Enhanced Thermal Properties by Chemical Liquid Deposition Methods. Propellants, Explosives, Pyrotechnics, 2012, 37, 597-604.	1.6	7
150	Solution-Processed Gas Sensors Based on ZnO Nanorods Array with an Exposed (0001) Facet for Enhanced Gas-Sensing Properties. Journal of Physical Chemistry C, 2012, 116, 10586-10591.	3.1	200
151	Influence of Dopants on Electrical Properties of ZnO-V2O5 Varistors Deduced from AC Impedance and Variable-Temperature Dielectric Spectroscopy. Journal of Electronic Materials, 2012, 41, 1970-1977.	2.2	16
152	A porous Cu/LDPE composite for copper-containing intrauterine contraceptive devices. Acta Biomaterialia, 2012, 8, 897-903.	8.3	20
153	Effect of Zinc Doping on Microstructures and Gas‣ensing Properties of <scp><scp>SnO<sub>2</sub></scp></scp> Nanocrystals. Journal of the American Ceramic Society, 2012, 95, 436-442.	3.8	27
154	A comparative study on UV light activated porous TiO2 and ZnO film sensors for gas sensing at room temperature. Ceramics International, 2012, 38, 503-509.	4.8	134
155	Comparison on photocatalytic degradation of gaseous formaldehyde by TiO2, ZnO and their composite. Ceramics International, 2012, 38, 4437-4444.	4.8	73
156	Indomethacin/Cu/LDPE porous composite for medicated copper intrauterine devices with controlled release performances. Composites Science and Technology, 2012, 72, 428-434.	7.8	13
157	Quantitative X-ray Rietveld analysis of metallic aluminum content in nano-aluminum powders. Materials Letters, 2012, 67, 177-179.	2.6	15
158	Synthesis of defect graphene and its application for room temperature humidity sensing. Materials Letters, 2012, 83, 76-79.	2.6	68
159	Visible-light activate mesoporous WO3 sensors with enhanced formaldehyde-sensing property at room temperature. Sensors and Actuators B: Chemical, 2012, 163, 260-266.	7.8	120
160	Nonisothermal crystallization behavior of Cu/LDPE nanocomposites prepared by solution blending method. Journal of Applied Polymer Science, 2012, 124, 3348-3356.	2.6	3
161	Study on the mechanical properties of Cu/LDPE composite IUDs. Contraception, 2011, 83, 255-262.	1.5	18
162	Improvement of gaseous pollutant photocatalysis with WO3/TiO2 heterojunctional-electrical layered system. Journal of Hazardous Materials, 2011, 196, 52-58.	12.4	49

#	Article	IF	CITATIONS
163	A Chinese liquor classification method based on liquid evaporation with one unmodulated metal oxide gas sensor. Sensors and Actuators B: Chemical, 2011, 160, 483-489.	7.8	20
164	Applied low bias with high frequency for enhancing mineralization ability of WO3 as visible-light-driven photocatalyst in gas phase. Catalysis Communications, 2011, 16, 180-183.	3.3	11
165	The sintering characteristics of pure tetrapod ZnO nanopowders prepared by thermal evaporation deposition (TED). Ceramics International, 2011, 37, 3469-3476.	4.8	10
166	Photoconductivity and trap-related decay in porous TiO2/ZnO nanocomposites. Journal of Applied Physics, 2011, 110, 123513.	2.5	26
167	An approach to give prospective life-span of the copper/low-density-polyethylene nanocomposite intrauterine device. Journal of Materials Science: Materials in Medicine, 2011, 22, 1773-1781.	3.6	19
168	Microwave sintering of ZnO nanopowders and characterization for gas sensing. Materials Science and Engineering B: Solid-State Materials for Advanced Technology, 2011, 176, 181-186.	3.5	7
169	Low bias photoelectrocatalytic (PEC) performance for organic vapour degradation using TiO2/WO3 nanocomposite. Applied Catalysis B: Environmental, 2011, 102, 157-162.	20.2	40
170	Nanostructural ZnO based coplanar gas sensor arrays from the injection of metal chloride solutions: Device processing, gas-sensing properties and selectivity in liquors applications. Sensors and Actuators B: Chemical, 2011, 153, 415-420.	7.8	22
171	C-doped WO3 microtubes assembled by nanoparticles with ultrahigh sensitivity to toluene at low operating temperature. Sensors and Actuators B: Chemical, 2011, 155, 86-92.	7.8	71
172	Microstructure and gas sensing properties of the ZnO thick film treated by hydrothermal method. Sensors and Actuators B: Chemical, 2010, 151, 107-113.	7.8	38
173	Research on the methods to determine metallic aluminum content in aluminum nanoparticles. Materials Chemistry and Physics, 2010, 120, 670-675.	4.0	32
174	Synthesis, formation mechanism and sensing properties of WO3 hydrate nanowire netted-spheres. Materials Research Bulletin, 2010, 45, 1541-1547.	5.2	41
175	Processing–structure–property relationships of Bi2WO6 nanostructures as visible-light-driven photocatalyst. Journal of Hazardous Materials, 2010, 183, 211-217.	12.4	58
176	Structural and photoelectrocatalytic characteristic of ZnO/ZnWO4/WO3 nanocomposites with double heterojunctions. Physica E: Low-Dimensional Systems and Nanostructures, 2010, 43, 503-509.	2.7	58
177	Fabrication and formaldehyde gas-sensing property of ZnO–MnO2 coplanar gas sensor arrays. Sensors and Actuators B: Chemical, 2010, 145, 457-463.	7.8	122
178	Controlled growth of SnO2 nanorods clusters via Zn doping and its influence on gas-sensing properties. Sensors and Actuators B: Chemical, 2010, 149, 336-344.	7.8	108
179	Quasiâ€Oneâ€Ðimensional Bismuth Tungsten Oxide Nanostructures Templated by Cotton Fibers. Journal of the American Ceramic Society, 2010, 93, 1479-1483.	3.8	12
180	Synthesis, formation mechanism and illuminated sensing properties of 3D WO3 nanowall. Journal of Alloys and Compounds, 2010, 495, 88-92.	5.5	41

#	Article	IF	CITATIONS
181	Enhanced visible light photocatalytic activity of QDS modified Bi2WO6 nanostructures. Catalysis Communications, 2010, 11, 1054-1057.	3.3	29
182	Characterization of Photoelectric Properties and Composition Effect of TiO <sub>2</sub> /ZnO/Fe <sub>2</sub> O <sub>3</sub> Composite by Combinatorial Methodology. ACS Combinatorial Science, 2010, 12, 883-889.	3.3	31
183	Synthesis of TiO <sub>2</sub> /WO <sub>3</sub> /MnO <sub>2</sub> Composites and High-Throughput Screening for Their Photoelectrical Properties. ACS Combinatorial Science, 2010, 12, 363-369.	3.3	36
184	Spoiling and formaldehyde-containing detections in octopus with an E-nose. Food Chemistry, 2009, 113, 1346-1350.	8.2	38
185	A sensor array optimization method for electronic noses with sub-arrays. Sensors and Actuators B: Chemical, 2009, 142, 243-252.	7.8	30
186	Detection and discrimination of low concentration explosives using MOS nanoparticle sensors. Journal of Hazardous Materials, 2009, 164, 1030-1035.	12.4	29
187	A reaction model of metal oxide gas sensors and a recognition method by pattern matching. Sensors and Actuators B: Chemical, 2009, 135, 552-559.	7.8	9
188	IDM release behavior and surface characteristics of the novel Cu/IDM/LDPE nanocomposite for intrauterine device. Colloids and Surfaces B: Biointerfaces, 2009, 69, 276-280.	5.0	9
189	Will ethylene oxide sterilization influence the application of novel Cu/LDPE nanocomposite intrauterine devices?. Contraception, 2009, 79, 65-70.	1.5	11
190	A Method of Feature Extraction on Recovery Curves for Fast Recognition Application With Metal Oxide Gas Sensor Array. IEEE Sensors Journal, 2009, 9, 1705-1710.	4.7	13
191	Effect of annealing temperature on the microstructures and photocatalytic property of colloidal ZnO nanoparticles. Journal of Physics and Chemistry of Solids, 2008, 69, 2440-2444.	4.0	46
192	â€~Sensory analysis' of Chinese vinegars using an electronic nose. Sensors and Actuators B: Chemical, 2008, 128, 586-593.	7.8	59
193	Zn2+ release behavior and surface characteristics of Zn/LDPE nanocomposites and ZnO/LDPE nanocomposites in simulated uterine solution. Journal of Materials Science: Materials in Medicine, 2008, 19, 3319-3326.	3.6	17
194	Microstructure and wear behaviour of laser-induced thermite reaction Al2O3 ceramic coatings on pure aluminum and AA7075 aluminum alloy. Journal Wuhan University of Technology, Materials Science Edition, 2008, 23, 89-94.	1.0	15
195	The effects of oxygen partial pressure on the microstructures and photocatalytic property of ZnO nanoparticles. Physica E: Low-Dimensional Systems and Nanostructures, 2008, 40, 2724-2729.	2.7	57
196	Formaldehyde sensor based on Ni-doped tetrapod-shaped ZnO nanopowder induced by external magnetic field. Physica E: Low-Dimensional Systems and Nanostructures, 2008, 41, 235-239.	2.7	41
197	An entire feature extraction method of metal oxide gas sensors. Sensors and Actuators B: Chemical, 2008, 132, 81-89.	7.8	52
198	Preparation and reactivity of aluminum nanopowders coated by hydroxyl-terminated polybutadiene (HTPB). Applied Surface Science, 2008, 254, 2413-2417.	6.1	65

#	Article	IF	CITATIONS
199	Effect of humidity on the gas sensing property of the tetrapod-shaped ZnO nanopowder sensor. Materials Science and Engineering B: Solid-State Materials for Advanced Technology, 2008, 149, 12-17.	3.5	93
200	Preparation and gas-sensing property of ZnO nanorod-bundle thin films. Materials Letters, 2008, 62, 2307-2310.	2.6	27
201	Effects of LDPE film on the properties of copper/LDPE composites for intrauterine contraceptive device. Materials Letters, 2008, 62, 4226-4228.	2.6	8
202	A Method of Feature Extraction From the Desorption Part of MOX's Response Curves to Gases. IEEE Sensors Journal, 2008, 8, 1816-1823.	4.7	14
203	Effect of implanted Cu/low-density polyethylene nanocomposite on the morphology of endometrium in the mouse. Fertility and Sterility, 2007, 88, 472-478.	1.0	20
204	The forces imposed by the novel T-shape Cu/LDPE nanocomposite intrauterine devices on the simulated uterine cavity. Contraception, 2007, 76, 326-330.	1.5	11
205	Activation of the calciumâ€added coal combustion solid residues. Asia-Pacific Journal of Chemical Engineering, 2007, 2, 177-181.	1.5	2
206	Cupric ion release controlled by copper/low-density polyethylene nanocomposite in simulated uterine solution. Journal of Biomedical Materials Research - Part B Applied Biomaterials, 2007, 80B, 220-225.	3.4	16
207	Electrochemical study of the corrosion behaviour of copper/low-density polyethylene microcomposite in the simulated uterine solution. Journal of Electroanalytical Chemistry, 2007, 603, 219-226.	3.8	2
208	Comparison of dye degradation efficiency using ZnO powders with various size scales. Journal of Hazardous Materials, 2007, 141, 645-652.	12.4	339
209	Formaldehydeâ€, Benzeneâ€, and Xyleneâ€Sensing Characterizations of Zn–W–O Nanocomposite Ceramics. Journal of the American Ceramic Society, 2007, 90, 3263-3267.	3.8	46
210	Characterization and thermal properties of carbon-coated aluminum nanopowders prepared by laser-induction complex heating in methane. Materials Letters, 2007, 61, 3211-3214.	2.6	56
211	A novel combustion method to prepare tetrapod nano-ZnO. Materials Letters, 2007, 61, 4603-4605.	2.6	13
212	Correlative investigation of copper/low-density polyethylene nanocomposite on the endometrial angiogenesis in rats. Frontiers of Medicine in China, 2007, 1, 401-404.	0.1	6
213	Characteristics and photocatalytic effects of Zn/ZnO nanowhiskers compared with ZnO nanoparticles. Journal Wuhan University of Technology, Materials Science Edition, 2007, 22, 643-648.	1.0	3
214	A feature extraction method and a sampling system for fast recognition of flammable liquids with a portable E-nose. Sensors and Actuators B: Chemical, 2007, 124, 437-443.	7.8	54
215	An alternate method of hierarchical classification for E-nose: Combined Fisher discriminant analysis and modified Sammon mapping. Sensors and Actuators B: Chemical, 2007, 127, 399-405.	7.8	13
216	Preparation and gas-sensing properties of Ce-doped ZnO thin-film sensors by dip-coating. Materials Science and Engineering B: Solid-State Materials for Advanced Technology, 2007, 137, 53-58.	3.5	229

#	Article	IF	CITATIONS
217	Structural characteristics and UV-light enhanced gas sensitivity of La-doped ZnO nanoparticles. Materials Science and Engineering B: Solid-State Materials for Advanced Technology, 2007, 141, 43-48.	3.5	78
218	Characterization of Chinese vinegars by electronic nose. Sensors and Actuators B: Chemical, 2006, 119, 538-546.	7.8	99
219	Using anti-VEGF McAb and magnetic nanoparticles as double-targeting vector for the radioimmunotherapy of liver cancer. Cancer Letters, 2006, 231, 169-175.	7.2	105
220	Corrosion characteristics of copper microparticles and copper nanoparticles in distilled water. Corrosion Science, 2006, 48, 3924-3932.	6.6	86
221	Labeling Polymeric Nanoparticles with Copper Chlorophyll as Contrast Agent for Electron Microscopy. Chemistry Letters, 2006, 35, 378-379.	1.3	0
222	Zn2+ release from zinc and zinc oxide particles in simulated uterine solution. Colloids and Surfaces B: Biointerfaces, 2006, 47, 140-145.	5.0	117
223	Novel 1–3 metal nanoparticle/polymer composites induced by hybrid external fields. Composites Science and Technology, 2006, 66, 1558-1563.	7.8	25
224	Electrochemical behaviour of copper/LDPE composites in the simulated uterine solution. Electrochimica Acta, 2006, 51, 5606-5611.	5.2	10
225	Effect of the loading and size of copper particles on the mechanical properties of novel Cu/LDPE composites for use in intrauterine devices. Materials Science & Engineering A: Structural Materials: Properties, Microstructure and Processing, 2006, 429, 329-333.	5.6	20
226	Laser grooving of Al2O3 plate by a pulsed Nd:YAG laser: Characteristics and application to the manufacture of gas sensors array heater. Materials Science & amp; Engineering A: Structural Materials: Properties, Microstructure and Processing, 2006, 435-436, 418-424.	5.6	9
227	Controlled organization of ZnO building blocks into complex nanostructures. Journal of Colloid and Interface Science, 2006, 297, 570-577.	9.4	45
228	Synthesis and characterization of ZnO nanostructures by two-step oxidation of Zn nano- and microparticles. Journal of Crystal Growth, 2006, 289, 663-669.	1.5	33
229	Controlled fabrication of nanostructured ZnO particles and porous thin films via a modified chemical bath deposition method. Journal of Crystal Growth, 2006, 291, 187-195.	1.5	64
230	Effect of molybdenum on continuous cooling bainite transformation of low-carbon microalloyed steel. Materials & Design, 2006, 27, 1169-1173.	5.1	73
231	Preparation, structure and thermal stability of Cu/LDPE nanocomposites. Materials Chemistry and Physics, 2006, 95, 122-129.	4.0	82
232	Influence of humidity on the thermal behavior of aluminum nanopowders. Materials Chemistry and Physics, 2006, 97, 127-131.	4.0	31
233	Electrical conductivity and gas sensitivity to VOCs of V-doped ZnFe2O4 nanoparticles. Materials Letters, 2006, 60, 1374-1378.	2.6	32
234	An attempt to directly trace polymeric nanoparticles in vivo with electron microscopy. Journal of Controlled Release, 2006, 115, 259-265.	9.9	15

#	Article	IF	CITATIONS
235	Polyacrylate-core/TiO2-shell nanocomposite particles prepared byin situ emulsion polymerization. Journal of Applied Polymer Science, 2006, 102, 1466-1470.	2.6	22
236	Water absorption characteristics of novel Cu/LDPE nanocomposite for use in intrauterine devices. Journal of Biomedical Materials Research - Part B Applied Biomaterials, 2006, 79B, 345-352.	3.4	13
237	ZnO Microspheres Self-assembled by Hexagonal Nanoplates. Chemistry Letters, 2005, 34, 260-261.	1.3	12
238	Controlled growth of ZnO by adding H2O. Journal of Crystal Growth, 2005, 277, 372-377.	1.5	72
239	Non-isothermal crystallization behavior of low-density polyethylene/copper nanocomposites. Thermochimica Acta, 2005, 427, 129-135.	2.7	40
240	Fractal dimension and photoluminescence of ZnO tetrapod nanowhiskers. Chemical Physics Letters, 2005, 406, 457-461.	2.6	41
241	A novel simplified method for preparing ZnO nanoneedles via H2O2 pre-oxidation. Materials Chemistry and Physics, 2005, 93, 539-543.	4.0	9
242	Corrosion behavior of copper/LDPE nanocomposites in simulated uterine solution. Biomaterials, 2005, 26, 2671-2676.	11.4	71
243	Identification and pattern recognition analysis of Chinese liquors by doped nano ZnO gas sensor array. Sensors and Actuators B: Chemical, 2005, 110, 370-376.	7.8	109
244	Polylactic acid nanoparticles targeted to brain microvascular endothelial cells. Journal of Huazhong University of Science and Technology [Medical Sciences], 2005, 25, 642-644.	1.0	1
245	Research on Cu2+ transformations of Cu and its oxides particles with different sizes in the simulated uterine solution. Corrosion Science, 2005, 47, 1039-1047.	6.6	36
246	Formation of tetrapod ZnO nanowhiskers and its optical properties. Materials Research Bulletin, 2004, 39, 637-645.	5.2	58
247	Specific role of polysorbate 80 coating on the targeting of nanoparticles to the brain. Biomaterials, 2004, 25, 3065-3071.	11.4	181
248	Microstructure transformation and interface structure of Co/Pt nano-multilayers prepared by ion beam sputtering deposition (IBSD). Surface and Coatings Technology, 2004, 176, 357-364.	4.8	3
249	Microstructure and electrical characteristics of ZnO–B2O3–PbO–V2O5–MnO2 ceramics prepared from ZnO nanopowders. Journal of the European Ceramic Society, 2004, 24, 3635-3641.	5.7	12
250	Optical absorptive characteristics of ZnO tetrapod nanowhiskers. Materials Letters, 2004, 58, 3792-3795.	2.6	7
251	The production and characteristics of solid lipid nanoparticles (SLNs). Biomaterials, 2003, 24, 1781-1785.	11.4	352
252	Condensation formation of Co–Fe nanoparticles and the related magnetic properties. Materials Letters, 2003, 57, 1539-1543.	2.6	6

#	Article	IF	CITATIONS
253	Morphological characteristic of Zn/ZnO nanopowders and the optical properties. Materials Science & Engineering A: Structural Materials: Properties, Microstructure and Processing, 2002, 328, 196-200.	5.6	36
254	The research on aggregation structure of PP materials under different condition and the influence on mechanical properties. Materials & Design, 2002, 23, 709-715.	5.1	4
255	Oxidation reaction during laser cladding of SAE1045 carbon steel with SiC/Cu alloy powder. Journal of Materials Science, 2001, 36, 1501-1505.	3.7	1
256	Corrosion resistance enhancement of Ni-resist ductile iron by laser surface alloying. Scripta Materialia, 2001, 44, 651-657.	5.2	12
257	Investigation of corrosion behavior of high nickel ductile iron by laser surface alloying with copper. Scripta Materialia, 2001, 44, 2747-2752.	5.2	13
258	The thermal physical formation of ZnO nanoparticles and their morphology. Journal of Crystal Growth, 2000, 217, 274-280.	1.5	81
259	Function of oxide film during the thermal oxidation process of Zn nanoparticles. Scripta Materialia, 2000, 43, 841-846.	5.2	20
260	Evaluation of alloy element redistribution within laser-melted layer. Surface and Coatings Technology, 1999, 113, 1-4.	4.8	9
261	Influence of deposition parameters on the internal stress in a-C:H films. Surface and Coatings Technology, 1999, 111, 141-147.	4.8	24
262	Structure transition comparison between the amorphous nanosize particles and coarse-grained polycrystalline of cobalt. Scripta Materialia, 1999, 11, 1061-1066.	0.5	51